

Radio Observations of GRB Host Galaxies

Elizabeth R. Stanway^{1*}, Andrew J. Levan¹ and Luke J. M. Davies^{2,3}

¹*Department of Physics, University of Warwick, Gibbet Hill Road, Coventry, CV4 7AL, UK*

²*H. H. Wills Physics Laboratory, University of Bristol, Tyndall Avenue, Bristol, BS8 1TL, UK*

³*ICRAR, The University of Western Australia, 35 Stirling Highway, Crawley, WA 6009, Australia*

ABSTRACT

We present 5.5 and 9.0 GHz observations of a sample of seventeen GRB host galaxies at $0.5 < z < 1.4$, using the radio continuum to explore their star formation properties in the context of the small but growing sample of galaxies with similar observations. Four sources are detected, one of those (GRB 100418A) likely due to lingering afterglow emission. We suggest that the previously-reported radio afterglow of GRB 100621A may instead be due to host galaxy flux. We see no strong evidence for redshift evolution in the typical star formation rate of GRB hosts, but note that the fraction of ‘dark’ bursts with detections is higher than would be expected given constraints on the more typical long GRB population. We also determine the average radio-derived star formation rates of core collapse supernovae at comparable redshift, and show that these are still well below the limits obtained for GRB hosts, and show evidence for a rise in typical star formation rate with redshift in supernova hosts.

Key words: galaxies: star formation – radio continuum: galaxies

1 INTRODUCTION

Long Gamma Ray Bursts (GRBs) are potentially a valuable probe of star forming galaxies. Arising from the core collapse of a massive star (e.g. Woosley & Heger 2006), they indicate the presence of recent star formation and are typically associated with the most intensely star forming region of their host galaxies (Fruchter et al. 2006; Svensson et al. 2010). Optical and ultraviolet observations of those hosts galaxies have suggested that these tend to be relatively low in metallicity (e.g. Graham & Fruchter 2013) and mass (e.g. Castro Cerón et al. 2010), with modest star formation rates (e.g. Christensen, Hjorth, & Gorosabel 2004; Savaglio, Glazebrook, & LeBorgne 2009). Thus they allow the selection and study of a galaxy population that may represent the low mass tail of the ultraviolet-selected, high redshift Lyman break galaxy luminosity function, and could plausibly dominate the ionising photon density of the Universe at early times (Chen et al. 2009; Tanvir et al. 2012).

If GRBs are an unbiased tracer of star formation, then they would be expected to occur in the galaxies dominating the star forming population at a given redshift. The phenomenon of ‘downsizing’ (Cowie et al. 1996) describes the tendency of star forming galaxies at low redshifts to be lower in mass, and also in metallicity, than the bulk of the galaxy population. Local radio surveys suggest that the majority of star formation at $z < 0.1$ occurs in a narrow range of

radio luminosities, corresponding to star formation rates of $1.5\text{--}15 M_{\odot} \text{ yr}^{-1}$ (Condon, Cotton, & Broderick 2002). More massive galaxies formed their stars at earlier times, typically at $z > 1$, and often at a higher specific star formation rate than is seen in the local Universe (see, for example, Cowie et al. 2004; Hopkins et al. 2010, and references therein). Thus the peak in the volume-averaged cosmic star formation rate, in AGN activity (indicative of co-evolution of spheroids) and in the number density of obscured starbursts such as submillimeter galaxies (Chapman et al. 2005) all occur at $z > 1$, and the mass and luminosity of a typical starburst decrease sharply towards $z = 0$.

However, there are indications that the host galaxies of GRBs do not necessarily trace this evolving, typical star forming population, but rather that the occurrence of a GRB may be likely in galaxies with certain physical properties regardless of redshift (see Levesque 2014, for a recent review). Extensive work in the optical and near-infrared has now produced a reasonably clear picture of the stellar populations in GRB hosts, in those examples sufficiently close to carry out a detailed analysis (e.g. Savaglio, Glazebrook, & LeBorgne 2009; Svensson et al. 2010) and in samples designed to have well understood completeness and selection effects (e.g. the ‘TOUGH’ sample, Hjorth et al. 2012; Michałowski et al. 2012).

By fitting the spectral energy distribution of a sample of host galaxies, Savaglio, Glazebrook, & LeBorgne (2009) found no evidence for evolution in host galaxy specific star formation rate or metallicity in the redshift interval $0 < z < 6$, although available metallicity information was

* E-mail: e.r.stanway@warwick.ac.uk

limited to damped Lyman- α system measurements at $z > 2$. Salvaterra et al. (2012) did find evidence for a strong evolution in either the luminosity or density distribution of GRB hosts and attributed this to a metallicity dependence in the GRB progenitor population.

While Svensson et al. (2010) did not consider redshift evolution, they compared GRB host locations to those of the core-collapse supernova population (which should also trace star formation) and found that the former occupy galaxies with higher optical surface brightness but less mass and smaller radii, as also suggested by Fruchter et al. (2006) and others. Work on supernovae themselves also support this. GRBs have been observationally associated with type Ic supernovae (Galama et al. 1998) but not with other types, and may well trace only a part of the Ic population, with additional constraints (e.g. on the progenitor rotation) necessary to generate a GRB. In local supernova samples, SNe Ic occur in more metal rich, exceptionally star forming galaxies, compared to the hosts of other core collapse supernovae (Kelly & Kirshner 2012), strengthening the case for GRBs picking out some subset of the full star forming galaxy population.

However this conclusion is by no means undisputed. As Coward et al. (2013) point out, a large number of observational selection effects as well as astrophysical biases must be taken into account. Initial suggestions that the GRB host population may show a sharp metallicity cut-off (e.g. Salvaterra et al. 2012; Kocevski, West, & Modjaz 2009) have been moderated by the detection of higher metallicity systems (e.g. Levesque et al. 2010a; Krühler et al. 2012) with a more gradual metallicity-dependent fall off in GRB rate now suggested (e.g. Kocevski & West 2011; Robertson & Ellis 2012, and references therein). While some recent studies conclude that GRBs show a pronounced aversion to high metallicity (e.g. Graham & Fruchter 2013), there are also those who believe no such dependence exists. Studies of the GRB host galaxy mass function and long GRB burst rate, based on a large sample observed by the GROND team, have suggested that no obvious biases in the host galaxy properties with metallicity, mass or redshift (Elliott et al. 2012) can be inferred, leaving this still very much an open question.

So, if the degree to which the properties of GRB hosts track those of the typical star forming galaxy at a given redshift is uncertain, converting a gamma ray burst rate to a volume averaged star formation density (and hence to the ionizing photon density vital for, amongst other things, hydrogen and helium reionisation) is fraught with difficulties and assumptions. Not only is the detection of bursts, their follow-up and redshift confirmation, rather an erratic process, with a difficult to establish completion function (see Fynbo et al. 2009; Hjorth et al. 2012; Krühler et al. 2012), but the derived star formation rates rely on prescriptions relating the observed death of a single massive star in each host galaxy to the stellar birth rate (e.g. Robertson & Ellis 2012).

Even studies to characterise GRB host samples in the optical are subject to their own selection biases, such as the possibility that some GRB host galaxies may be characterised by a significant quantity of dust and obscured star formation and hence omitted. Early sub-millimeter and radio observations suggested that as many as a third of

GRBs could arise in these dusty and relatively massive systems (Berger et al. 2003; Priddey et al. 2006; Tanvir et al. 2004). The definition of a population of ‘Dark GRBs’ with low optical emission relative to their X-ray flux (Jakobsson et al. 2004) again strengthened earlier suggestions that dust extinction may play a role that must be understood in the interpretation of these sources (e.g. see discussion in Groot et al. 1998; Djorgovski et al. 2001; Rol et al. 2005; Cenko et al. 2009; Greiner et al. 2011, and references therein). Including this ‘dark’ population leads to determining a much higher average dust content in the GRB host population than previously believed, but is still insufficient to explain the early submillimeter results (Perley et al. 2013). Studies of the lowest redshift bursts (Stanway, Davies, & Levan 2010) and other more recent work (e.g. Hunt et al. 2014; Perley & Perley 2013; Michałowski et al. 2012; Wang, Chen, & Huang 2012) has suggested that the typical GRB host galaxy does not in fact host large quantities of extinguished star formation.

As a result, samples of GRBs with measured radio fluxes remain small, with early work focused on detailed studies of individual targets (e.g. Kohno et al. 2005; Michałowski et al. 2009; Stanway et al. 2011). Recent work by Michałowski et al. (2012) represented a substantial improvement in the sample of GRB hosts observed in the radio, presenting observations for 22 $z < 1$ sources, including those derived from the ‘TOUGH’ sample (Hjorth et al. 2012) and sources compiled from the literature. Of these, three were detected. While the constraints placed on individual sources varied significantly from object to object, a stacking analysis based on the median redshift of the sample suggested that the typical undetected source may be relatively low in star formation rate ($\text{SFR} < 15 M_{\odot} \text{ yr}^{-1}$) and have dust extinction ($A_{2800\mu\text{m}} < 6.7 \text{ mag}$).

Recent improvements in correlator bandwidth, and hence sensitivity, at the major radio observatories has opened up the potential to change this, with observations reaching star formation rates within a factor of a few of the optical and ultraviolet derived values for GRB hosts now achievable with a reasonable investment of time. In this paper we extend the radio analysis of long GRB hosts to higher redshifts, and increase the number of observed sources, aiming to characterise their star formation without assumptions regarding their redshift evolution. We use the radio continuum to explore the star formation rates of the GRB host galaxies in our sample, in the context of the small but growing number of galaxies with similar observations. We present 5.5 and 9.0 GHz observations of seventeen GRB host galaxies at $z = 0.5 - 1.4$. Of these, radio observations of twelve sources are reported here for the first time. Of the remaining sources, four have previously been observed at ~ 1.4 GHz (Michałowski et al. 2012). We report 5.5 GHz flux constraints and significantly improve the observed star formation rate limits in two cases, and present a tentative (2.3σ) detection at 5.5 GHz of a third source. For the final source we report a flux limit consistent with the detection reported by Perley & Perley (2013).

In section 2 we introduce observations, taken at both the Australia Telescope Compact Array (ATCA) and the Jansky Very Large Array (VLA). In section 3 we examine the two most recent bursts in detail and establish interpretation as afterglow or star formation. In section 4 we discuss

the conversion from radio flux to star formation rate. In section 5 we discuss our results in the context of previous work in this field, before presenting our conclusions in section 6.

Throughout, optical magnitudes are presented in the AB system. Host galaxies are typically referred to by the name of the associated GRB, but measurements are those of the host galaxy unless otherwise specified. Where necessary, we use a standard Λ CDM cosmology with $H_0 = 70 \text{ km s}^{-1} \text{ Mpc}^{-1}$, $\Omega_M = 0.3$ and $\Omega_\Lambda = 0.7$.

2 OBSERVATIONS

2.1 Sample Selection

Gamma ray bursts were selected from the data compilation table¹ recording burst triggers from the *Swift* telescope (Gehrels et al. 2004). The primary criterion for sample selection was the existence of a known redshift for the GRB or its host galaxy, with sufficient precision to accurately derive rest-frame properties, and sufficiently low to allow useful radio constraints.

As mentioned below and discussed in section 5.3, one initial goal of our ATCA programme (see section 2.2) was to evaluate whether ‘dark bursts’ differed in their radio properties from the wider population. As a result four of the sources in this study were identified as dark bursts (lying at $z = 0.5 - 0.8$), and other long GRBs at similar redshifts were preferentially selected for our ATCA observations so as to allow more direct comparison of their properties. The targets for our VLA observations (section 2.3) were chosen to lie at slightly higher redshifts, ideally at $z = 1.0 - 1.4$, to extend this work to earlier times and take best advantage of the higher sensitivity of the VLA.

Southern sources were prioritized so as to maximize coverage of the uv -plane in interferometric radio telescopes. If multiple targets satisfied these selection criteria and were accessible to the telescope during the observing programme, then the sources observed were selected at random. As a result, and given the patchy spectroscopic follow-up of bursts (particularly in the early years of the *Swift* mission), the sample is unlikely to be complete, but nonetheless samples the known population. All sources all satisfy the $T_{90} > 2.0 \text{ s}$ criterion for a ‘long’ duration gamma-ray burst (where T_{90} is the interval within which 90% of the integrated counts from the burst are detected Kouveliotou et al. 1993).

Our primary source for redshift information was the compilation provided in the *Swift* burst lookup table². This table is hosted by Swift and seeks to compile data on these triggers and their follow up from GCN announcement and other sources, although its data is occasionally superseded by more detailed analyses. For two sources in our sample, GRB 060814 and GRB 071003, two highly discrepant redshifts appear in the literature.

GRB 071003 was initially reported as lying at $z = 1.10$ due to the presence of an absorption line system in the afterglow at this redshift (Perley et al. 2007). However reexamination of the afterglow spectrum revealed the presence of a weaker but convincingly detected line system at $z = 1.604$

(Perley et al. 2008). This latter redshift is now the accepted value for this burst. While we initially selected this source for observation based on the lower redshift, we adopt the better supported value of $z = 1.60$ for the analysis in this paper.

GRB 060814 was selected for follow-up based on the $z = 0.84$ interpretation given in the *Swift* burst table, derived from Keck spectroscopy (Thoene, Perley, & Bloom 2007) at early times and appearing in several catalog papers (e.g. Kann et al. 2010). However later observations have suggested that the faint host galaxy was misidentified and a second redshift $z = 1.92$ was reported, from line detections in a star forming galaxy determined to be closer to the burst location (Salvaterra et al. 2012; Krühler et al. 2012). Throughout, we give results for the $z = 1.92$ hypothesis based on the higher probability that this is the host galaxy redshift. We note that the measured flux limit would correspond to a substantially lower star formation rate if $z = 0.84$ is used instead (as figure 2 illustrates). If this target were detected, it would also be subject to some uncertainty as to whether the flux arose from the GRB host, or the intervening $z = 0.84$ galaxy. Due to the likely high redshift (which renders comparison with the rest of our sample problematic) and degree of ambiguity, this source is omitted from statistical analyses in section 5.

2.2 ATCA Observations

Radio continuum observations of 13 GRB host galaxies were undertaken in 2011 April 15-19 using the Australia Telescope Compact Array (ATCA)³. The targets for this programme were selected as *Swift*-detected long gamma-ray bursts lying at $z \sim 0.5 - 0.8$, based on published observations. Four targets were included which satisfy the conditions for being defined as ‘Dark GRBs’ (i.e. optically faint, see section 5.3).

Data were taken simultaneously at 5.5 and 9.0 GHz, with a correlator bandwidth of 2 GHz centered on each frequency. The telescope was in its most elongated 6A configuration, with maximum and minimum baselines of 5.938 and 0.337 km respectively, aligned East-West, and earth rotation synthesis was used to improve coverage of the uv -plane. Data were taken across the full range of possible hour angles, with a total on-source integration time per target of ~ 140 minutes. A bright, compact source close on the sky to each target was used for phase calibration, and absolute flux and bandpass calibration were determined through observations of PKS 1934-638 (the standard calibrator for ATCA).

Data were reduced using the standard software package MIRIAD (Sault et al. 1995), applying appropriate bandpass, phase and flux calibrations, and after flagging the dataset for radio frequency interference. Each band comprised 2048 channels, each of 1 MHz bandwidth. Multi-frequency synthesis images were constructed using natural weighting and the full bandwidth between the flagged edges of each band. The resulting synthesised beam depends on uv -plane coverage. This tends to be relatively poor for northern sources, so the beam is elongated in declination as given in table 1. The targets were placed

¹ http://swift.gsfc.nasa.gov/archive/grb_table/

² http://swift.gsfc.nasa.gov/archive/grb_table/

³ Observations associated with programme C2544

close to the centre of the 8.5 arcmin primary beam. Given their redshifts and the typical identification of GRB hosts as relatively low mass galaxies (e.g. Svensson et al. 2010; Savaglio, Glazebrook, & LeBorgne 2009) our GRB host targets were expected to be compact or point sources in these observations. In each image, multiple faint sources were detected, and the images were ‘cleaned’ using standard prescriptions.

The resulting 5.5 GHz synthesis images were inspected for any flux excess in close proximity to the burst or its host galaxy (where known). The typical uncertainty in the enhanced *Swift* XRT position for the burst (Evans et al. 2009) is 1.4 arcseconds, with a few cases where the constraints are poorer (~ 3 arcsec). In four fields, a flux excess exceeding the typical image noise by a factor of two were observed within the XRT error circle, or coincident with a known host galaxy. Either incomplete sampling of the *uv*-plane or the presence of a bright object close to the telescope beam can lead to flux being scattered across a synthesised image in a correlated noise pattern. We inspected each target to ensure that there was no sign of large scale pattern noise that might explain a flux excess at the target location.

In order to rigorously determine the 5.5 GHz flux (or limit) for each target and its associated uncertainty, we made use of the MIRIAD task ‘imfit’, specifying that the software attempt to fit a point source, matching the dimensions of the synthesised beam. In order to allow the most conservative limit on the host galaxy flux (i.e. the maximum value permitted by the data), we permitted the algorithm to search around the XRT position by up to twice the width of the elongated synthesised beam in Right Ascension and a beam width in declination, sufficient to encompass both the XRT error circle and any plausible uncertainty associated with bandwidth smearing or the telescope pointing algorithm. This typically resulted in a search box of $\sim 10 \times 3''$, and a measured offset of peak flux from the provided coordinates of < 2 arcseconds.

For non-detections, we report the maximum permitted point source flux and its associated error (scaled by the software to account for correlated noise), based on this procedure in table 1. These represent conservative limits. The scaled errors, which account for the difficulty in determining a flux excess above the structured background noise exceed the image root-mean-square noise (often quoted as a flux uncertainty) by a factor > 5 .

For the four sources with an identified flux excess within the search region, we explored the possibility of fitting an extended source, resulting in a poorer fit to the data in all four cases. In each case, ‘imfit’ returned a position consistent with the peak flux identified by visual inspection of the images. For consistency, and based on the large synthesised beam of the telescope at these frequencies, we report the point source flux for these objects together with the reported estimate of uncertainty in table 1, and present 5.5 GHz radio maps of these objects in figure 1.

Of these objects, two (GRBs 100621A and 100418A) are well defined, clear radio detections coincident with the GRB X-ray location. A third (GRB 050223) shows a significant (3σ) point source coincident with the host galaxy identified by (Pellizza et al. 2006). The fourth source (GRB 060729) presents an excess of 2.3σ over the background noise, coincident with the burst location.

While marginal as a claimed detection, this flux excess remains when the data is sub-divided, or a different weighting is used for image reconstruction. In addition to being coincident with the X-ray location, the flux excess is stronger than any of the likely noise features in its vicinity on the image, and is not straightforwardly attributable to the beam pattern extending from any other object. The probability of a noise fluctuation of this strength occurring in our search region by chance is 3%. In our sample of 17 sources (combining ATCA targets with the VLA observations discussed in section 2.3) we might expect 0.5 such fluctuations (assuming gaussian statistics). We note that no targets in our sample show a negative flux of comparable significance. Thus, while it remains possible that this radio flux is not attributable to the target, in the analysis that follows, we treat the measured 5.5 GHz flux as a radio detection, with the caveat that it might also be treated as a robust upper limit.

Observations at 9.0 GHz are more sensitive to atmospheric conditions and yield less sensitive constraints on star formation rate for all but the most peculiar of radio spectral slopes. We nonetheless inspect our 9.0 GHz for targets coincident with the GRB locations, using the same procedure described above. Two of the 5.5 GHz-detected sources were also detected at 9.0 GHz. The remaining sources showed no evidence for a 9.0 GHz detection.

We note that the constraints obtained above may be weakened if the sources are extended relative to the synthesised beam. The median effective radius of GRB host galaxies is ~ 1.7 kpc (Wainwright, Berger, & Penprase 2007). This corresponds to a projected size of just $0.3''$ at $z = 0.5$ and $0.2''$ at $z = 1.0$. Of 47 GRB hosts in the Wainwright, Berger, & Penprase (2007) sample, only one (GRB 011121 at $z = 0.34$) would be comparable to a $1.5''$ beam size in our imaging. While it is possible that a more extended host may exist within our relatively small sample, such studies of archival space-based imaging suggest that this is unlikely.

2.3 VLA Observations

The survey was extended to higher redshifts ($z = 1.0 - 1.6$) through the observation of four additional sources at the Karl G. Jansky Very Large Array (VLA). Observations were obtained in service mode in June-July 2012 and were associated with programme 12A-279 (PI: Stanway). A total bandwidth of 2 GHz was centred at 5.5 GHz, with data collected in 1024 channels, each 2 MHz in width. Observations were performed in B configuration.

Three targets - GRBs 071003, 080413B and 091208B - were each observed for ~ 80 minutes on source, and a fourth target - GRB 100901A - for ~ 160 minutes. As in the case of the ATCA observations above, a nearby point source was used for phase calibration on each target and absolute flux calibration was provided by the standard calibrator 3C48. Data were flagged and reduced using standard CASA tasks, producing a multi-frequency synthesis image for each target, using natural weighting. Both the improved instantaneous *uv*-plane coverage and the northern location of the VLA relative to the ATCA led to a more compact synthesised beam in these observations, as shown in table 1.

Each image revealed a number of faint radio sources, as well as known catalogue sources. In the field of GRB 071003,

Object ID	location (J2000)	z	5.5 GHz Flux $\mu\text{Jy}/\text{beam}$	S/N	Beam size	SFR $\text{M}_{\odot} \text{yr}^{-1}$	9.0 GHz Flux $\mu\text{Jy}/\text{beam}$
GRB 081007	22:39:50.49 -40:08:49.1	0.529	38.1 ± 26.7		$3.9 \times 2.2''$	< 35	
GRB 060729	06:21:31.79 -62:22:12.4	0.54	65.4 ± 27.8	2.3	$4.1 \times 1.8''$	55 ± 24	60 ± 41
GRB 100621A	21:01:13.10 -51:06:22.8	0.542	120.1 ± 31.9	3.8	$3.5 \times 2.2''$	101 ± 27	106 ± 42
GRB 090424	12:38:05.12 +16:50:15.4	0.544	36.6 ± 28.0		$10 \times 1.7''$	< 38	
GRB 050223	18:05:32.35 -62:28:19.7	0.591	90.5 ± 30.1	3.0	$3.3 \times 2.0''$	93 ± 31	93 ± 48
GRB 050525A	18:32:32.64 +26:20:21.6	0.606	15.6 ± 33.8		$8.4 \times 1.6''$	< 53	
GRB 100418A	17:05:27.19 +11:27:39.8	0.623	363.0 ± 48.0	7.6	$18 \times 1.6''$	—	199 ± 57
GRB 051022	23:56:04.11 +19:36:23.7	0.809	23.0 ± 35.5		$14 \times 1.5''$	< 98	
GRB 070508	20:51:11.80 -78:23:05.1	0.82	35.0 ± 28.2		$4.3 \times 1.6''$	< 101	
GRB 071112C	02:36:50.95 +28:22:16.7	0.823	50.1 ± 25.2		$7.3 \times 1.6''$	< 126	
GRB 050824	00:48:56.20 +22:36:32.9	0.83	42.3 ± 33.2		$10 \times 1.5''$	< 111	
GRB 080710	00:33:05.63 +19:30:05.5	0.845	42.6 ± 28.8		$11 \times 1.6''$	< 112	
GRB 060814	14:45:21.32 +20:35:09.2	1.92	43.6 ± 23.5		$9.1 \times 1.6''$	< 670	
GRB 091208B	01:57:34.10 +16:53:22.9	1.063	0.0 ± 4.2		$1.3 \times 1.1''$	< 33	
GRB 080413B	21:44:34.60 -19:58:51.8	1.101	7.6 ± 4.7		$1.9 \times 1.0''$	< 39	
GRB 100901A	01:49:03.41 +22:45:30.1	1.408	0.2 ± 2.9		$1.2 \times 1.1''$	< 42	
GRB 071003	20:07:24.11 +10:56:51.1	1.604	2.1 ± 4.3		$1.4 \times 0.9''$	< 83	

Table 1. Results from the radio observations at 5.5 and 9.0 GHz, taken at the ATCA and VLA. Objects are ordered by redshift, with the exception of GRB 060814 (see section 3). Fluxes and 1σ uncertainties are given in $\mu\text{Jy}/\text{beam}$. The beam size is given at 5.5 GHz and is half this size at 9.0 GHz. For measurements with an associated $S/N > 2$, the signal to noise is shown in the fourth column. The penultimate column gives the inferred star formation rate in solar masses per year, assuming the radio flux is driven by star formation, as described in section 4, with 2σ limits where appropriate. The detection of GRB 100418A is not interpreted as star formation (see section 3). If GRB 060814 is instead placed at $z = 0.84$ (see section 2.1), the limit instead corresponds to $\sim 107 \text{M}_{\odot} \text{yr}^{-1}$. For sources detected at 5.5 GHz, the final column gives the observed-frame 9.0 GHz flux in μJy . No other sources are detected at 9.0 GHz. The final four sources were observed at the VLA, and 9.0 GHz data was not taken. Locations are given for the GRB afterglow and taken from the *Swift* XRT enhanced positions catalogue.

we recover the known NVSS galaxy J200658+110024 at a separation of 7.3 arcmin from our target. As before, we permit a small search region, allowing for the X-ray position uncertainty, any pointing uncertainty or offsets between the GRB or its host. None of the four targeted sources were individually detected. Given the non-detection, we measure the flux within the GRB error circle, allowing for small ($< 2''$) shifts in the centroid if these maximise the flux, thus achieving the most conservative constraints. Our resulting sensitive flux limits as shown in table 1 and figure 2.

3 AFTERGLOW OR HOST GALAXY?

The majority of the targets in this survey were observed a substantial time (> 2 years) after the initial burst. However, in two cases - GRBs 100418A and 100621A - radio fluxes were obtained less than a year post-burst in the galaxy rest-frame. Given that these sources are two of only four detections in our sample, the question arises: are we observing host galaxy flux, or are our observations contaminated by the late time radio afterglow of the burst itself?

We explore this possibility through archival imaging and the literature. It has been established that GRB 100621A was unusually bright. Greiner et al. (2013) analysed the multi-wavelength afterglow properties, including observations taken with ATCA in Jun-Jul 2010 (4-27 days after burst) at the same frequencies as those observed here. In table 2 we report the fluxes measured by Greiner et al. (2013) and compare with those measured in our observations. Greiner et al. suggested that their 2010 Jul 17 observations (measured at 17 days post-burst in the rest frame) might suggest a rapid fall off of the afterglow, or that the early time data might be explained by scintillation.

The radio afterglow of long GRBs can be observed across an extended period of time. Unlike the optical afterglow, which typically fades on a time scale of hours, radio afterglows extend across days or months. The timescales for this afterglow depend on the observed frequency, since high frequency flux peaks earlier than low frequency flux. Chandra & Frail (2012) compiled data on 95 GRBs for which there were radio detections spanning from minutes to ~ 500 days following the *Swift* gamma-ray trigger. In 63 cases there was sufficient data to determine a peak flux epoch for at least one radio frequency. Only two sources have radio afterglows peaking at > 50 days at ~ 5 GHz or higher, with the vast majority peaking at < 10 days. Typical sources show a fall in flux of more than an order of magnitude between the first few days and a rest frame epoch of 200 days post-burst, with the flux evolution at 8.5 GHz being consistent with $f(t) \propto t^{-1}$ for times after peak flux.

Our late time observations of GRB 100621A are entirely consistent with those measured almost 200 days earlier in the galaxy rest frame. The 2010 July observation remains discrepant but we note that this was also the noisiest observation, and given the large errors, the results are still consistent within 2σ of our measured value. Since the initial claim of a fading radio afterglow hinged entirely on this relatively noisy datapoint, our late time observation suggests that such an interpretation should be reconsidered.

We cannot rule out an afterglow hypothesis, and further observations would be required to do so. However, given the lack of evidence for fading or other significant time variation in this source at either 5.5 or 9.0 GHz, we suggest that the constant flux is at least as likely to arise from underlying star formation in the host galaxy, rather than the burst afterglow. We make this assumption in the analysis that fol-

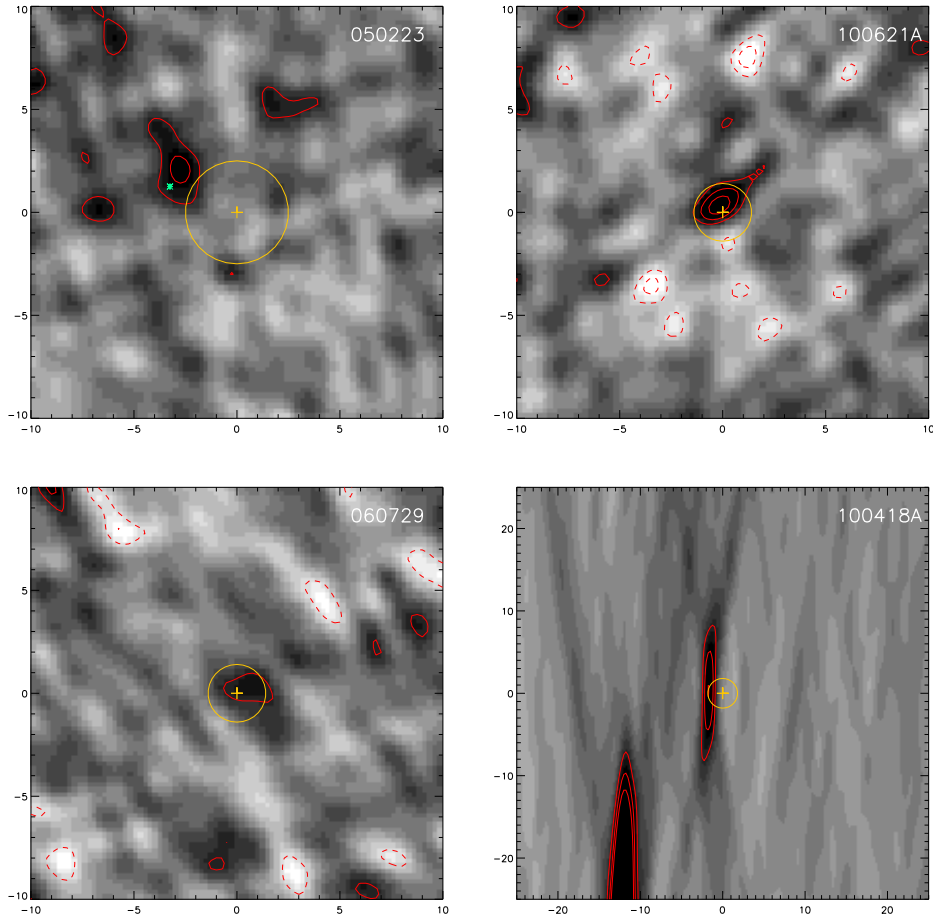


Figure 1. 5.5 GHz radio maps of the four detections identified in table 1. We note again that the detection of the host of GRB 060729 is very tentative, at 2.3σ . Dark colours indicate higher fluxes, and contours are indicated at ± 2 , 3 and 4 times the image noise level. The yellow cross and circle mark the *Swift* XRT location identified for the afterglow and its associated error circle. In the case of GRB 050223, the second cross indicates the position of the host galaxy identified by Pellizza et al. (2006), with which the radio detection appears to be associated. Axes are labelled in arcsecond offsets from the XRT location, with North up. Note that the synthesised beam for GRB 100418A is very extended in declination, as shown in table 1.

lows, while noting that it is inevitably subject to debate. Combining all available ATCA data in a single image (and thereby improving *uv*-plane coverage and sensitivity), we determine a best 5.5 GHz flux for the host of GRB 100621A of $142 \pm 19 \mu\text{Jy}$, corresponding to a star formation rate of $119 \pm 16 M_{\odot} \text{ yr}^{-1}$ (well within the range of star formation rates seen for the GRB population, see next section) - consistent with each of the reported individual measurements to within their errors. The source appears to be a point source at the resolution of the $3.2 \times 1.5''$ synthesised beam.

The radio afterglow behaviour of GRB 100418A has also been subject to previous investigation, with a campaign of long term follow-up conducted by (Moin et al. 2013). In figure 3, we place our observation in the context of that study. Interestingly, our independent observation, taken with ATCA, confirms the relatively high flux measured at the VLA twelve days before (in the observer frame). This might suggest a puzzling late time rebrightening of this source at ~ 200 days post burst trigger in the rest frame. Whatever the implication of this high flux measurement, it seems clear that the flux in this system is unlikely to be

Date	Time post burst	5.5 GHz flux	9.0 GHz flux
2010 Jun 24-25	1.6	137 ± 17	150 ± 28
2010 Jun 25-26	2.3	129 ± 24	127 ± 45
2010 Jul 17	17	-43 ± 85	49 ± 100
2011 Apr 18	195	120 ± 32	106 ± 42

Table 2. ATCA observations of GRB 100621A including those presented here for the first time, and those reported by Greiner et al. (2013). Fluxes and 1σ flux errors (measured for a point source at the burst location) are given in $\mu\text{Jy}/\text{beam}$. Time after the *Swift* GRB trigger is given in days, calculated in the source *rest frame* (observed frame / 1.5).

dominated by emission from the GRB host galaxy and so cannot be interpreted as arising from star formation.

4 STAR FORMATION RATES

The radio continuum flux from a galaxy can be converted to a star formation rate, assuming that the emission is

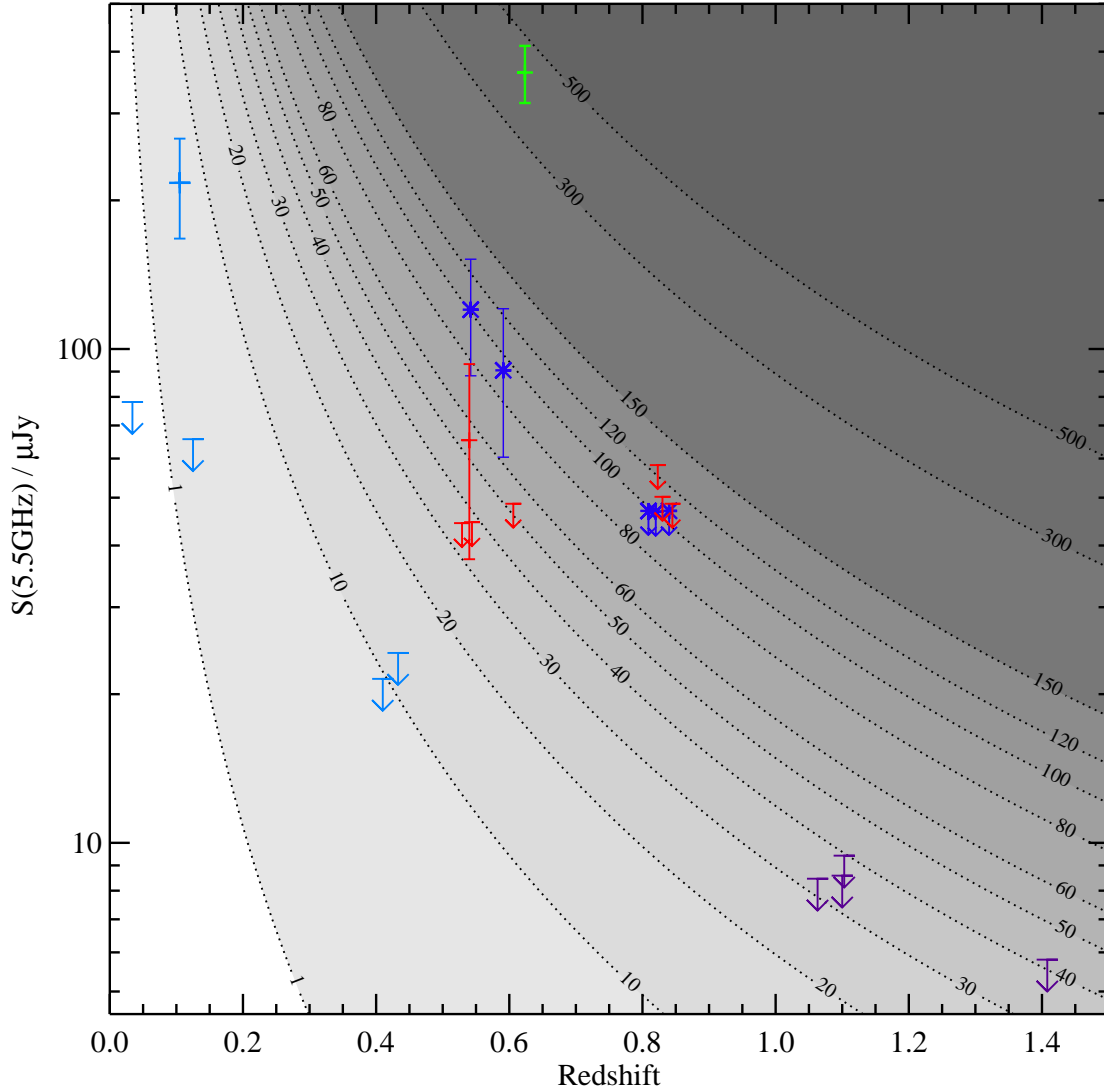


Figure 2. The measured fluxes (or 2σ limits thereon) of the samples discussed in this paper. The four points at $z > 1$ are derived from VLA data, the remaining points from ATCA data. The five points at $z < 0.5$ are those presented in Stanway et al (2010) and are shown to provide a point of comparison. The five observations targeting the location of ‘dark’ bursts are indicated by asterisks (two detections, three limits). The contours indicate inferred radio-continuum-derived star formation rates in solar masses per year, as discussed in section 4. We note that the highest flux detection, that of GRB 100418A, should not be interpreted in terms of star formation as discussed in section 3. GRB 060814, at $z = 1.92$, is omitted from this figure for clarity.

dominated by the synchrotron component, which is emitted by electrons accelerated in supernovae and their remnants. Given that these events occur at the end of the life of massive stars, the establishment of radio continuum emission shows a delay relative to the ultraviolet emission from young starbursts, but is directly related to star formation in older populations with ongoing star formation.

Star formation rates determined for GRB host galaxies based on optical-near-infrared emission are typically relatively low, of order $1\text{--}10 M_{\odot} \text{yr}^{-1}$ and are derived either from fitting to the spectral energy distribution or to some assumed conversion factor from ultraviolet continuum or $H\alpha$ line emission (e.g. Savaglio, Glazebrook, & LeBorgne 2009; Levesque et al. 2010a; Krühler et al. 2011). However the in-

ferred star formation rate from fitting to the UV-optical provides information primarily about the often blue, relatively young star forming population dominating the emission at these wavelengths, and does not provide any useful constraint on the fraction of star formation taking place in obscured regions. A relevant example is that of GRB 100621A, which has a measured obscuration from the burst itself of $A_V = 3.8$, while a fit to the SED of the host yields just $A_V = 0.6$ (Krühler et al. 2011). The star formation associated with the burst clearly occurred in, or behind, a heavily obscured region, and the optical data are not representative of this extinguished population.

Since radio wavelengths are less affected by dust extinction than the ultraviolet and optical, we might expect this

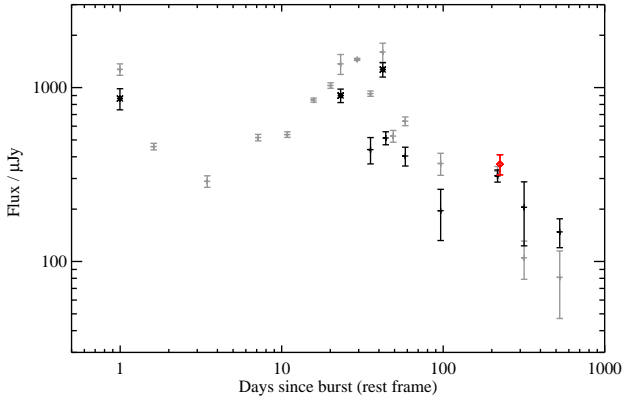


Figure 3. ATCA and VLA observations of GRB 100418A placing the observation reported here in the context of the radio afterglow light-curve reported by Moin et al. (2013). Fluxes and 1σ flux errors (measured for a point source at the burst location) are given in $\mu\text{Jy}/\text{beam}$. Observations at ~ 5.5 GHz are shown in black (asterisks: 5.5 GHz from ATCA, crosses: 4.9 GHz from VLA). Data at higher frequency ($\sim 7 - 9$ GHz) is shown in grey. The 5.5 GHz flux reported here is shown in red. Time after the *Swift* GRB trigger is given in the source rest frame.

flux to be a more complete measurement of the galaxy star formation rate, and to exceed the optically-derived values if substantial quantities of dust are present in the host galaxy.

We convert our measured 5.5 GHz fluxes to star formation rates, using the known redshift of the sources, and the conversion prescription of Berger et al. (2003) and Yun & Carilli (2002) which depends on observed frequency, source redshift, and radio spectral slope, α .

Following Berger et al., we set $\alpha = -0.6$, appropriate for faint radio sources. Using a steeper spectral slope, $\alpha = -0.75$, results in star formation rate estimates 25% higher but does not significantly affect our conclusions. We fix the dust temperature and emissivity index at $T_d = 58$ K and $\beta = 1.35$ respectively (again for comparison with previous studies). The derived star formation rates (in $M_\odot \text{yr}^{-1}$), are relatively insensitive to these dust parameters for observations at ~ 1 -10 GHz.

We over-plot contours on figure 2 to show the star formation rates equivalent to the given 5.5 GHz flux as a function of redshift. The last column in table 1 gives the inferred star formation rate (or limit thereon) in solar masses per year for each object, based on our 5.5 GHz observations, assuming that the observed radio flux is attributable to star formation. The measurement of GRB 100418A is not interpreted as star formation, as discussed in section 3.

Given the very different beam shapes and sensitivities of the ATCA data, we do not attempt to stack undetected sources. However we do stack our three undetected sources with VLA data at $z \sim 1.1$. No source is detected in our stack, which has an rms flux of $1.9 \mu\text{Jy}$, limiting the mean star formation rate of these three galaxies to $< 16 M_\odot \text{yr}^{-1}$ (2σ).

We note that, while the host of GRB 050223 is detected at 3.4 and 4.6 μm , none of the objects in our sample are detected in 22 μm *W4*-band infrared data from the ALLWISE data release (Wright et al. 2010; Mainzer et al. 2011). Flux

Target	λ_{rest} μm	Flux mJy	SFR $M_\odot \text{yr}^{-1}$
GRB 050223	13.8	< 1.9	< 320
GRB 060729	14.3	< 2.2	< 290
GRB 100418A	13.6	< 1.2	< 220
GRB 100621A	14.3	< 2.4	< 320

Table 3. WISE limits on observed 22 μm (*W4*) flux and inferred star formation rate for the four sources with possible radio detections. 2σ limits are given in each case.

in the long wavelength WISE bands is also excited by star formation and can be used as a star formation rate indicator, although this relies on calibrations that have been determined locally, and will vary as a function of redshift. At the redshift of our four detected sources, the 22 μm is probing the rest frame region around 14 μm - and so is sensitive to hot dust and PAH emission. While strong flux in this region is indicative of a strong photon source - often star formation - the conversion is dependent on the physical properties of the star formation region and is thus poorly calibrated. WISE is also a relatively shallow survey, sufficient to identify very luminous sources, but not typical star forming galaxies at $z > 0.5$. In table 3, we give flux limits and equivalent star formation rate estimates for the four sources with proposed radio detections in this work. We apply the star formation rate conversion factor calculated from $z = 0 - 0.3$ galaxies (Lee, Hwang, & Ko 2013) for luminosities measured in the broad *W3* filter, which spans 11-16 μm (observed) and thus provides a better calibration for our distant sources than the low redshift *W4* band. As can be seen, the limits obtained by WISE are consistent with our inferred radio star formation rates for these sources, and also consistent with none of the larger sample being heavily obscured, submillimeter galaxy-like intense starbursts.

An additional constraint exists for one of our detected sources - the host of GRB 050223 - in the form of mid-infrared *Herschel Space Telescope* data. Hunt et al. (2014) observed a small sample of ‘dark’ GRBs with the PACS and SPIRE instruments, obtaining constraints on their mid-infrared spectral energy distribution (SED). In the case of GRB 050223, the host galaxy remained undetected, and the SED fit is driven by the optical to near-infrared data observed through to the WISE *W1* and *W2* bands. As figure 2 of Hunt et al. (2014) makes clear, the *Herschel* data do not tightly constrain the SED of this target, and derived parameters such as dust temperature and emission spectrum, star burst fraction, star formation rate and obscuration are highly degenerate. In the case of GRB 050223 the fit to the stellar spectrum dominated optical does little to break these degeneracies or constrain the longer wavelength emission. Indeed the infrared star formation rate determined by these authors is somewhat puzzling, actually falling below that estimated from the (uncorrected) ultraviolet emission. Given that this host galaxy had already been identified as a dusty starburst, with an $A_V > 2$ (i.e. extinguished by a factor > 5 in the ultraviolet, Pellizza et al. 2006), one might expect an estimate of the infrared emission to exceed the ultraviolet estimate by this factor, even without accounting for any more obscured emission. Thus while noting that our estimate of star formation significantly exceeds that of Hunt et al., we

suggest that this indicates that further investigation of this source, or a revision to the existing spectral energy distribution fits, might be appropriate.

5 DISCUSSION

5.1 Redshift Evolution

In figure 4 we consider the GRB host star formation rate measurements and limits derived from radio emission, as a function of lookback time. In addition to the data reported in this paper and our previous work (Stanway, Davies, & Levan 2010), we also plot the radio-derived star formation rates reported and compiled by Michałowski et al. (2012). To enable direct comparison, we adjust the star formation rates of Michałowski et al. (2012) to account for the steeper radio spectral slope assumed in that paper, and to report 2σ limits where a source is undetected.

In total, figure 4 includes data on 40 long gamma ray burst host galaxies. Of these, a mere six have secure detections (excluding the afterglow of GRB 100418A), and two of those lie at $z < 0.15$ (i.e. 2 Gyr lookback time), making clear the difficulty of observing these low mass, moderately star forming galaxies over substantial intervals of cosmic time.

Five sources have only modest constraints (a 2σ limit on star formation rate $>200 M_{\odot} \text{ yr}^{-1}$) and a sixth source is detected with a very high star formation rate ($\sim 400 M_{\odot} \text{ yr}^{-1}$). This source, GRB 021211 is a pre-*Swift* burst, arguably with different selection criteria and characteristics to the bulk of the sample. We note that the high flux density for this source ($S_{1.4\text{GHz}} = 330 \pm 31 \mu\text{Jy}$) reported by Michałowski et al. (2012) is inconsistent with that reported by (Hatsukade et al. 2012), who constrain the star formation rate to $\lesssim 60 M_{\odot} \text{ yr}^{-1}$ (2σ , with our assumptions). Further investigation of this source is clearly needed.

In summary, no more than 5 of the 40 ($12 \pm 6\%$) GRB hosts with radio constraints, have star formation rates exceeding $200 M_{\odot} \text{ yr}^{-1}$. This confirms, and indeed strengthens, the findings of Michałowski et al. (2012) who analysed data on about half of this composite sample, and is somewhat lower than suggested by early, pre-*Swift* and higher redshift work by Berger et al. (2003, who suggested a fraction of 20%) and Tanvir et al. (2004, who detected 3 of 21 sources). The reasons for this remain unclear, although small number statistics and the selection criteria for follow-up targets no doubt contribute to the discrepancy.

The detection fraction in our $z \sim 0.5$ (lookback time ~ 5.5 Gyr) ATCA observations is perhaps slightly higher than might be expected based on the the statistics of the sample as a whole. Of nine GRB hosts at $0.45 < z < 0.70$ with star formation rate limits better than $200 M_{\odot} \text{ yr}^{-1}$ we detect three sources ($33 \pm 19\%$). While these statistics are still based on small numbers of objects, if they were typical of the sample as a whole we might have expected several more detections outside this redshift range, including more examples at $z < 0.5$ and perhaps one of our $z \sim 1$ targets.

At present, the number counts in this subsample are insufficient to extrapolate further, and we note that one of these is our least significant detection. However, it suggests that further investigation may be warranted to determine

whether this anomaly resolves with added data, or remains statistically significant. If there is, in fact, a redshift dependence in the typical star formation rate of GRB host galaxies, then it is possible that $z \sim 0.5$ may represent a sweet spot in current telescope sensitivity relative to the typical star formation rate in GRB host galaxies. At lower redshifts, GRBs may be occurring in galaxies with lower typical star formation rates, while at higher redshift, the current radio limits are too weak to reliably probe this regime.

We note that other than this anomaly, there is at best very modest evidence for redshift evolution in the radio derived star formation rates in individual GRB host galaxies. The measurement sample is dominated by upper limits at all redshifts, but these are less constraining with increasing redshift. Nonetheless the upper limits on typical sources at lookback times of 6-10 Gyrs (roughly corresponding to $z = 0.65 - 1.85$) constrain the typical GRB host radio-derived star formation rate to be no more than an order of magnitude higher than that observed at $z < 0.15$. This is comparable to the expected change in the typical star formation rate for galaxies of a given mass over the same interval due to the effects of downsizing (see, for example, Speagle et al. 2014, and references therein), and so while we limit the redshift evolution of GRB hosts, the current sample is insufficient to conclude that their evolution is significantly different to that of typical star forming galaxies over cosmic time.

5.2 Core Collapse SN Hosts

Long GRBs are believed to be generated by the breakout of relativistic jets during the collapse of of a massive star at the end of its life (Woosley & Heger 2006). They have been observed to be coincident with Type Ic supernovae, and may be associated with core collapse supernovae (CCSN) more generally (see Fruchter et al. 2006, and references therein).

However, as discussed in section 1, Fruchter et al. (2006) found that GRB hosts are typically less optically luminous than those of CCSNe, and also that the transient is more closely associated with the peak of the light distribution in the host, based on optical photometry with the *Hubble Space Telescope*. They suggested that this might well represent a difference in the metallicity of the progenitor population, with GRBs biased towards the most massive and lowest metallicity stellar populations. This conclusion was broadly supported by Svensson et al. (2010), who employed template fitting of the spectral energy distribution of the host galaxies to make the same comparison. However Svensson et al. (2010) concluded that the difference between the two host populations was less pronounced in the blue optical bands which are dominated by star formation. This suggests the intriguing possibility that in the star formation-dominated radio continuum, the two populations may again appear similar.

We consider the published catalogue of core-collapse SNe in the GOODS field (Strolger et al. 2004; Dahlen, Strolger, & Riess 2008; Dahlen et al. 2012), matching that also analysed by Svensson et al. (2010) and omitting only sources without radio coverage. These sources were initially selected, based on detection of the optical supernova, to lie in the two GOODS survey fields due to their extensive multi-wavelength coverage with *HST*

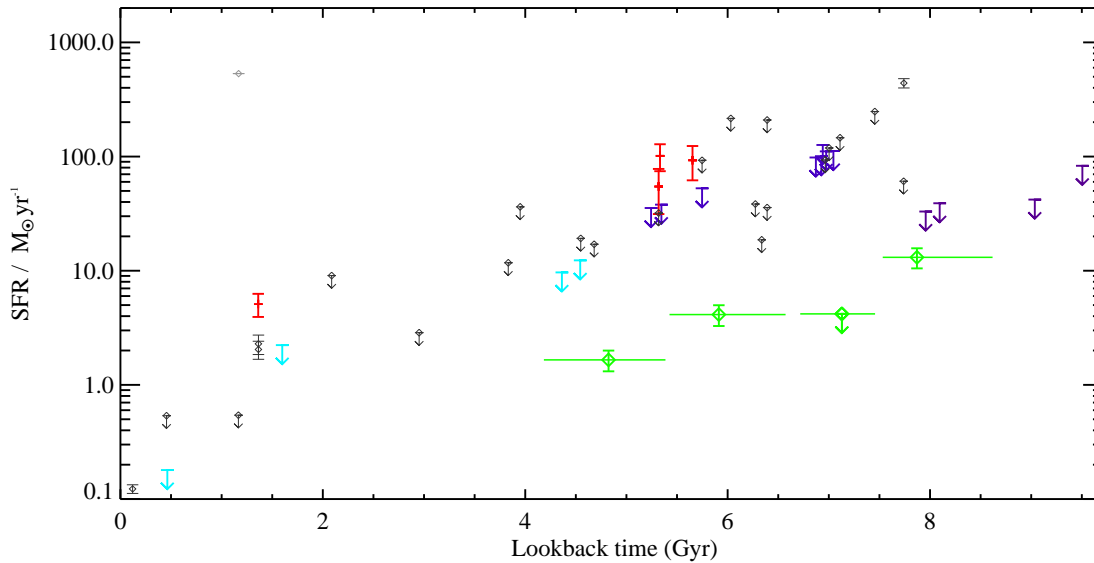


Figure 4. The radio-inferred star formation rates (and limits) for GRB host galaxies with radio observations, shown as a function of lookback time. Large symbols indicate 5.5 GHz measurements taken as part of this programme from Stanway, Davies, & Levan (2010) at $z < 0.5$ (lookback < 5 Gyr), and from the observations presented in this paper from ATCA ($0.5 < z < 1.0$, $5-7.5$ Gyr) and the VLA ($z > 1$, > 7.5 Gyr). Small symbols indicate the measurements reported or compiled by Michałowski et al. (2012) - triangles mark measurements at < 5 GHz and diamonds those at higher frequency. Note that several sources have measurements at multiple frequencies, so not every point is independent. All limits are at the 2σ level. Large green diamonds indicate the average rates inferred for the hosts of core collapse SNe in the GOODS fields as described in section 5.2, with horizontal bars showing the limits of each redshift bin. GRB 060814 lies at $z = 1.92$ and is omitted from this figure.

(Giavalisco et al. 2004). Both GOODS fields have also been surveyed with deep radio imaging at 1.4 GHz from the VLA. We make use of the publically released maps of GOODS-S from Miller et al. (2008) and GOODS-N from Morrison et al. (2010). Both images have a comparable sensitivity, and are on the same pixel scale. While several core collapse SN hosts show a marginal detection, no individual source is strongly detected. We combine the radio flux at the location of those CCSN in the sample that lie within the appropriate image to produce stacked images, taking the mean pixel value at each point.

We divide the sample of CCSN in Svensson et al. (2010) into four redshift bins, each with $\Delta z = 0.2$, and combine the objects in each separately. The resulting stacked images are shown in figure 5 and their measured properties given in table 4. Radio properties of individual GOODS supernova hosts are given in the appendix and not discussed further here. In three redshift bins the average CCSN host galaxy is well detected. The $z \sim 0.85$ sample has no clear detection, and the measured flux is treated as an upper limit.

The GOODS-S field was observed by the VLA in Jun-Sep 2007, > 2 years after the last supernova was detected and host galaxy measurements are unlikely to be contaminated by residual flux from the supernovae. The GOODS-N observations represent a combination of data from 1996 and Feb 2005-Apr 2006. We cannot rule out the contribution of supernova flux to these observations, but note that $\sim 78\%$ of the GOODS-N data were collected either before the SNe were detected, or > 1 year post-SN. The radio lightcurves of core-collapse supernovae decay on comparable timescales to those of GRBs but are typically at least two orders of

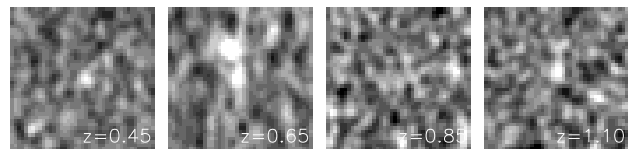


Figure 5. The stacked radio flux at 1.4 GHz for core collapse SN hosts in the GOODS fields, as described in section 5.2. The average CCSN host is well detected in three redshift bins. The third bin, centred at $z \sim 0.85$ does not show any evidence for a detection and is treated as an upper limit. The bright off-centre source in the $z \sim 0.65$ stack is the result of bright neighbours in two individual images biasing the mean.

magnitude less luminous than GRBs at comparable redshift (Kamble et al. 2014). Given the typical peak radio luminosity of 2×10^{27} ergs s^{-1} Hz $^{-1}$ and a time decay of index ~ -1 (Weiler et al. 2002), we would expect radio supernovae to have dropped well below our stacked detection limit within a year in the observed frame, at all redshifts considered here. Assuming then that the host galaxy flux dominates over any supernova contribution, we convert the fluxes to star formation rates, using the same prescription given earlier to account for the different observed-frame frequency of the observations (1.4 GHz rather than 5.5 GHz).

The derived star formation rates are compared to those of the GRB host sample and shown as large green diamonds in figure 4. The CCSNe typically occur in galaxies with lower star formation rates than are reached by current samples, confirming that the scarcity of detections in our sample is unsurprising. Interestingly, however, the results of the core

$\langle z \rangle$ (Range)	Number	Flux _{1.4 GHz} / μJy	SFR / $M_{\odot} \text{ yr}^{-1}$
0.47 (0.35-0.55)	17	6.0 ± 1.2	1.7 ± 0.3
0.63 (0.55-0.75)	17	7.6 ± 1.6	4.1 ± 0.9
0.86 (0.75-0.95)	8	3.8 ± 1.9	< 4.2
1.04 (0.95-1.15)	9	7.9 ± 1.6	13.1 ± 2.6

Table 4. The number of sources and measured radio properties of the CCSN host galaxy stacks discussed in section 5.2.

collapse supernovae host sample are consistent with an increase in the typical radio-derived star formation rate in these galaxies with increasing redshift.

This behaviour appears consistent with the expected picture of cosmic ‘downsizing’ (Cowie et al. 1996). Not only does the volume-averaged star formation density of the Universe increase by more than an order of magnitude with increasing lookback time from $z = 0$ to $z = 1$ but the size and star formation rate of galaxies in the star-forming population also increases. Thus, if core-collapse supernova rate is directly proportional to star formation rate (i.e. the larger core collapse population is an unbiased tracer, as GRBs are not believed to be), the majority of events would be expected to be seen in more intense starbursts at $z \sim 1$ than typically exist in the local Universe. As a result the detection of a single core-collapse supernova implies the existence of more young stars if it occurs at $z \sim 1$ than if it occurs more locally, and any attempt to reconstruct the cosmic star formation history would require an adjustment for this evolution in the host galaxy population.

If GRBs are indeed still more biased towards low metallicity environments, as theoretically and observationally suggested (e.g. Woosley & Heger 2006; Levesque et al. 2010a; Graham & Fruchter 2013), but not universally accepted (e.g. Levesque et al. 2010b), then this effect would likely be stronger, with lower star formation rates needed, on average, to produce a burst at high redshift than in the local Universe, since a fraction of the higher metallicity star formation is not represented in the GRB rate. Further observations are clearly required to determine whether GRB hosts follow a similar pattern to that seen in the small sample of CCSN presented here, which could plausibly bias attempts to interpret the burst rate at a given redshift as a proxy for the volume averaged cosmic star formation rate. We note that the increase in radio-derived star formation rate between our lowest redshift bin and the highest is a factor of $7.7^{+3.5}_{-2.5}$. If the typical rates seen in GRBs in the local Universe increase by a similar factor, it would be doubtful whether our radio observations are sufficiently sensitive to detect them.

In a pessimistic scenario, where GRB hosts are no more radio luminous than those of the larger CCSN population at high redshift, securing radio detections at the level of the core collapse supernovae hosts would require an improvement in sensitivity by a factor of 10 over the current observations. While using a larger array (for example the VLA rather than ATCA) may allow progress to be made in reasonable integration times at $z \sim 0.5$, the hosts at $z \sim 1$ will need integration times approaching 8-10 hours per source to reach star formation rates of $\sim 10 M_{\odot} \text{ yr}^{-1}$, making this an expensive study to undertake.

5.3 Dark GRB Hosts

Four of our sample, GRBs 051022, 060814, 050223 and 100621A, have been identified as dark bursts in earlier work. These are defined as sources which are sub-luminous in the optical relative to the X-ray, typically with an optical-to-X-ray spectral slope $\beta_{OX} < 0.5$. This spectral index is beyond those normally allowed in GRB fireball models, and is most commonly attributed to the presence of dust in the GRB host galaxy. Indeed, the majority of these dark bursts have been shown to be associated with high optical extinctions (Perley et al. 2013). Studies in the optical and near-infrared have suggested that the hosts of such bursts are typically more massive and chemically evolved than those of other GRBs, with higher star formation rates (e.g. Perley et al. 2013; Krühler et al. 2011). However, as already discussed, dust obscuration can make interpretation of galaxy spectral energy distributions challenging. Given the difficulties associated with faint optical emission, radio continuum observations have the potential to improve our understanding of the host galaxies of these sources (Zauderer et al. 2013).

Two of our candidates, GRBs 051022 and 060814 are included in the dark burst sample of Perley et al. (2013). Another, GRB 050223, does not satisfy the strict criteria for β_{OX} , with the strongest available constraint of $\beta_{OX} < 0.8$, but based on its host galaxy properties Pellizza et al. (2006) claim this source as part of the dark sample (although Page et al. 2005, find no evidence for excess extinction in the X-ray emission from the burst). A high extinction ($A_V=3.8$) and low $\beta_{OX} = 0.278$ has also been reported for a fourth source, GRB 100621A (Krühler et al. 2011; Melandri et al. 2012).

Radio constraints on the host galaxies of an exclusively ‘dark’ sample of 15 hosts, observed from the VLA, have recently been presented by Perley & Perley (2013). Only one source, GRB 051022, overlaps with the sample presented here, with the majority of targets in the Perley & Perley study lying at higher redshift than those in our sample. Four of their targets were detected: 3 host galaxies at $\text{SFR} > 800 M_{\odot} \text{ yr}^{-1}$ and GRB 051022 at $74 \pm 20 M_{\odot} \text{ yr}^{-1}$, consistent with our limit given in table 1. Two further host galaxies (GRBs 060202 and 090417B) were constrained to have radio star formation rates under $120 M_{\odot} \text{ yr}^{-1}$, while the remaining, higher redshift targets, have less constraining upper limits on their star formation rates spanning from < 325 to a relatively weak $< 4140 M_{\odot} \text{ yr}^{-1}$.

We detect the hosts of dark GRBs 050223 and 100621A in our 5.5 GHz observations, giving radio-derived star formation rates of $\sim 90 - 100 M_{\odot} \text{ yr}^{-1}$ – significantly higher than the majority of GRB hosts. Given the likely high redshift of GRB 060814 (see section 2.1), the star formation rate constraint on this source is rather weak and we exclude it from further discussion.

Between the Perley & Perley (2013) study and the observations reported here, the hosts of nine dark bursts have detected or well constrained radio derived SFRs - three in the range $\text{SFR} \sim 70100 M_{\odot} \text{ yr}^{-1}$, three with higher star formation rates more akin to ULIRGs ($> 200 M_{\odot} \text{ yr}^{-1}$), and three undetected sources constrained to have $\text{SFR} < 120 M_{\odot} \text{ yr}^{-1}$ (typical of the GRB host population as a whole, see figure 4). The remainder (lying at higher redshift) have relatively weak constraints on their radio flux and could still

be harbouring star formation rates of several hundred solar masses per year, and yet remain undetected. As with GRBs 060814, we exclude these from further analysis.

To evaluate the probability of this detection rate occurring by chance, assuming that dark burst hosts are drawn from the same underlying star formation rate distribution as the non-dark burst sample, we consider a bootstrap re-sampling of the full existing, non-dark burst, dataset. The observations presented here and in Michałowski et al. (2012) provide detections or limits of $< 120 M_{\odot} \text{ yr}^{-1}$ or better on 28 individual non-dark sources. We make the conservative assumption that we have barely missed detecting the majority of sources (i.e. that their 2σ limits are representative of their true star formation rates), and randomly draw subsamples of nine objects from this compilation to mimic the dark burst sample, repeating the process 10^7 times. We find that in only 1.7% of cases do six or more randomly sampled objects in a sample of nine have star formation rates exceeding $60 M_{\odot} \text{ yr}^{-1}$. As such, it is highly unlikely that the dark bursts we have identified above, are drawn from same underlying population as the non-dark bursts. The deviation of dark burst host star formation rates from those of the non-dark GRBs, is significant at the 2σ level (subject, of course, to the vagaries of low number statistics) and merits further investigation.

This may suggest that while, as Perley & Perley (2013) and others have concluded, dark GRB hosts are typically forming stars at a lower rate than submillimeter galaxies, they are nonetheless biased towards systems with higher star formation rates than seen in the general, less extinguished long GRB host population.

6 CONCLUSIONS

Our conclusions can be summarized as follows:

(i) We present observations of 17 gamma ray burst host galaxies at 5.5 GHz, with 13 of these also observed simultaneously at 9.0 GHz. Typical rms noise levels in the images are $\sim 30 \mu\text{Jy}/\text{beam}$.

(ii) Radio continuum (5.5 GHz) point sources are detected at the location of four GRBs (GRB 050223, 060729, 100418A and 100621A). Assuming a standard conversion factors, the fluxes of these correspond to radio-derived star formation rates of $\sim 60 - 200 M_{\odot} \text{ yr}^{-1}$.

(iii) Comparison of our late time measurements with published data suggests that the radio flux reported at early times by Greiner et al. (2013) in GRB 100621A likely arises from the host galaxy rather than the burst afterglow as previously suggested. However our detection of GRB 100418A likely arises from late time radio afterglow emission. Our remaining two sources are observed several years post-burst.

(iv) Based on our observations, we see no strong evidence for evolution in the typical star formation rate of the GRB host galaxy population with redshift, but note that we detect three sources at $z \sim 0.5$ - an anomalously high fraction of sources in that redshift bin. Given the small number statistics it is difficult to comment further on the significance of this.

(v) We compare to the typical radio emission of CCSN hosts from the GOODS survey, securing detections in stacked samples at $z \sim 0.47, 0.63$ and 1.04, but not at

$z \sim 0.86$. These detections correspond to star formation rates that are substantially lower (by an order of magnitude) than current GRB host limits. They also show some evidence for a trend towards higher star formation rates at higher redshift.

(vi) Four of our targets satisfy criteria for identification as dark bursts. We detect two of these. In combination with earlier results, we suggest that these sources may have average star formation rates rather higher than those seen in the general population of long GRB hosts.

ACKNOWLEDGMENTS

This paper is based in part on data obtained at the Australia Telescope Compact Array associated with programme C2544. The Australia Telescope Compact Array is part of the Australia Telescope National Facility which is funded by the Commonwealth of Australia for operation as a National Facility managed by CSIRO.

Also based in part on observations taken at the NRAO Karl G. Jansky Very Large Array (VLA), associated with programme 12A-279. The National Radio Astronomy Observatory is a facility of the National Science Foundation operated under cooperative agreement by Associated Universities, Inc.

This work made use of data supplied by the UK Swift Science Data Centre at the University of Leicester (Evans et al. 2009). We also made use of Ned Wright's very useful cosmology calculator (Wright 2006).

AJL and ERS acknowledge support from the UK Science and Technology Facilities Council, under the Warwick Astrophysics consolidated grant ST/L000733/1 and PATT-linked travel support grant. We also acknowledge the influence of suggestions from the anonymous referee on the evolution of this paper.

REFERENCES

- Berger E., Cowie L. L., Kulkarni S. R., Frail D. A., Aussen H., Barger A. J., 2003, *ApJ*, 588, 99
- Castro Cerón J. M., Michałowski M. J., Hjorth J., Malesani D., Gorosabel J., Watson D., Fynbo J. P. U., Morales Calderón M., 2010, *ApJ*, 721, 1919
- Cenko S. B., et al., 2009, *ApJ*, 693, 1484
- Chandra P., Frail D. A., 2012, *ApJ*, 746, 156
- Chapman S. C., Blain A. W., Smail I., Ivison R. J., 2005, *ApJ*, 622, 772
- Chen H.-W., et al., 2009, *ApJ*, 691, 152
- Christensen L., Hjorth J., Gorosabel J., 2004, *A&A*, 425, 913
- Condon J. J., Cotton W. D., Broderick J. J., 2002, *AJ*, 124, 675
- Coward D. M., Howell E. J., Branchesi M., Stratta G., Guetta D., Gendre B., Macpherson D., 2013, *MNRAS*, 432, 2141
- Cowie L. L., Songaila A., Hu E. M., Cohen J. G., 1996, *AJ*, 112, 839
- Cowie L. L., Barger A. J., Fomalont E. B., Capak P., 2004, *ApJ*, 603, L69
- Dahlen T., Strolger L.-G., Riess A. G., 2008, *ApJ*, 681, 462

- Dahlen T., Strolger L.-G., Riess A. G., Mattila S., Kankare E., Mobasher B., 2012, *ApJ*, 757, 70
- Djorgovski S. G., Frail D. A., Kulkarni S. R., Bloom J. S., Odewahn S. C., Diercks A., 2001, *ApJ*, 562, 654
- Elliott J., Greiner J., Khochfar S., Schady P., Johnson J. L., Rau A., 2012, *A&A*, 539, A113
- Evans P. A., et al., 2009, *MNRAS*, 397, 1177
- Fruchter A. S., et al., 2006, *Nature*, 441, 463
- Fynbo J. P. U., et al., 2009, *ApJS*, 185, 526
- Galama T. J., et al., 1998, *Natur*, 395, 670
- Gehrels N., et al., 2004, *ApJ*, 611, 1005
- Giavalisco M., et al., 2004, *ApJ*, 600, L93
- Graham J. F., Fruchter A. S., 2013, *ApJ*, 774, 119
- Greiner J., et al., 2011, *A&A*, 526, A30
- Greiner J., et al., 2013, *A&A*, 560, A70
- Groot P. J., et al., 1998, *ApJ*, 493, L27
- Hatsukade B., Hashimoto T., Ohta K., Nakanishi K., Tamura Y., Kohno K., 2012, *ApJ*, 748, 108
- Hao J.-M., Yuan Y.-F., 2013, *ApJ*, 772, 42
- Hjorth J., et al., 2012, *ApJ*, 756, 187
- Hopkins P. F., Younger J. D., Hayward C. C., Narayanan D., Hernquist L., 2010, *MNRAS*, 402, 1693
- Hunt L. K., et al., 2014, *arXiv*, arXiv:1402.4006
- Jakobsson P., Hjorth J., Fynbo J. P. U., Watson D., Pedersen K., Björnsson G., Gorosabel J., 2004, *ApJ*, 617, L21
- Kamble A., Soderberg A., Berger E., Zauderer A., Chakraborti S., Williams P., 2014, *arXiv*, arXiv:1401.1221
- Kann D. A., et al., 2010, *ApJ*, 720, 1513
- Kelly P. L., Kirshner R. P., 2012, *ApJ*, 759, 107
- Kocevski D., West A. A., 2011, *ApJ*, 735, L8
- Kocevski D., West A. A., Modjaz M., 2009, *ApJ*, 702, 377
- Kohno K., et al., 2005, *PASJ*, 57, 147
- Kouveliotou C., Meegan C. A., Fishman G. J., Bhat N. P., Briggs M. S., Koshut T. M., Paciesas W. S., Pendleton G. N., 1993, *ApJ*, 413, L101
- Krühler T., et al., 2011, *A&A*, 534, A108
- Krühler T., et al., 2012, *arXiv*, arXiv:1205.4036
- Lee J. C., Hwang H. S., Ko J., 2013, *ApJ*, 774, 62
- Levesque E. M., 2014, *PASP*, 126, 1
- Levesque E. M., Kewley L. J., Berger E., Zahid H. J., 2010a, *AJ*, 140, 1557
- Levesque E. M., Kewley L. J., Graham J. F., Fruchter A. S., 2010b, *ApJ*, 712, L26
- Mainzer A., et al., 2011, *ApJ*, 731, 53
- Melandri A., et al., 2012, *MNRAS*, 421, 1265
- Michałowski M. J., et al., 2012, *ApJ*, 755, 85
- Michałowski M. J., et al., 2009, *ApJ*, 693, 347
- Miller N. A., Fomalont E. B., Kellermann K. L., Mainieri V., Norman C., Padovani P., Rosati P., Tozzi P., 2008, *ApJS*, 179, 114
- Moin A., et al., 2013, *ApJ*, 779, 105
- Morrison G. E., Owen F. N., Dickinson M., Ivison R. J., Ibar E., 2010, *ApJS*, 188, 178
- Nakagawa Y. E., et al., 2006, *PASJ*, 58, L35
- Page K. L., et al., 2005, *MNRAS*, 363, L76
- Pellizza L. J., et al., 2006, *A&A*, 459, L5
- Perley D. A., et al., 2013, *ApJ*, 778, 128
- Perley D. A., et al., 2008, *ApJ*, 688, 470
- Perley D. A., Chornock R., Bloom J. S., Fassnacht C., Auger M. W., 2007, *GCN*, 6850, 1
- Perley D. A., Perley R. A., 2013, *ApJ*, 778, 172
- Priddey R. S. et al, 2006, *MNRAS*, 369, 1189
- Robertson B. E., Ellis R. S., 2012, *ApJ*, 744, 95
- Rol E., Wijers R. A. M. J., Kouveliotou C., Kaper L., Kaneko Y., 2005, *ApJ*, 624, 868
- Salvaterra R., et al., 2012, *ApJ*, 749, 68
- Sault, R. J., Teuben, P. J., & Wright, M. C. H. 1995, *Astronomical Data Analysis Software and Systems IV*, 77, 433
- Savaglio S., Glazebrook K., LeBorgne D., 2009, *ApJ*, 691, 182
- Speagle J. S., Steinhardt C. L., Capak P. L., Silverman J. D., 2014, *arXiv*, arXiv:1405.2041
- Stanway E. R., Davies L. J. M., Levan A. J., 2010, *MNRAS*, 409, L74
- Stanway E. R., Bremer M. N., Tanvir N. R., Levan A. J., Davies L. J. M., 2011, *MNRAS*, 410, 1496
- Strolger L.-G., et al., 2004, *ApJ*, 613, 200
- Svensson K. M., Levan A. J., Tanvir N. R., Fruchter A. S., Strolger L.-G., 2010, *MNRAS*, 405, 57
- Svensson K. M., et al., 2012, *MNRAS*, 421, 25
- Tanvir N. R., et al., 2004, *MNRAS*, 352, 1073
- Tanvir N. R., et al., 2012, *ApJ*, 754, 46
- Thoene C. C., Perley D. A., Bloom J. S., 2007, *GCN*, 6663
- Wainwright C., Berger E., Penprase B. E., 2007, *ApJ*, 657, 367
- Wang W.-H., Chen H.-W., Huang K.-Y., 2012, *ApJ*, 761, L32
- Weiler K. W., Panagia N., Montes M. J., Sramek R. A., 2002, *ARA&A*, 40, 387
- Wirth G. D., et al., 2004, *AJ*, 127, 3121
- Woolley S. E., Heger A., 2006, *ApJ*, 637, 914
- Wright E. L., 2006, *PASP*, 118, 1711
- Wright E. L., et al., 2010, *AJ*, 140, 1868
- Yun M. S., Carilli C. L., 2002, *ApJ*, 568, 88
- Zauderer B. A., et al., 2013, *ApJ*, 767, 161

This paper has been typeset from a \TeX / \LaTeX file prepared by the author.

APPENDIX A: THE HOSTS OF CORE COLLAPSE SUPERNOVAE

As discussed in section 5.2, we extract radio fluxes at the locations of core-collapse supernovae originally identified as part of the GOODS campaign (Giavalisco et al. 2004). Sources identified during the 2002-2003 observing campaign were catalogued, classified and reported by Strolger et al. (2004), listed both by ‘nickname’ and IAU approved transient name. Sources from 2004-2005 were classified by and discussed in Dahlen, Strolger, & Riess (2008) and Dahlen et al. (2012). Formal IAU naming was not sought for these later objects. Spectroscopic redshifts were obtained either from literature values for the supernova host galaxy or through Keck Observatory spectroscopy primarily originating from or compiled by the Team Keck Treasury Redshift Survey (Wirth et al. 2004). Target classifications, locations and redshifts for all these sources were made available electronically in 2008, as described in Dahlen, Strolger, & Riess (2008), and we make use of this publically released catalogue, and specifically those supernovae classified as core collapse and within the coverage region of the available radio imaging.

In this appendix we tabulate the measured radio

fluxes at each position in table A1. Radio fluxes are measured on the publically released 1.4 GHz VLA maps of GOODS-S from Miller et al. (2008) and GOODS-N from Morrison et al. (2010). Names presented are those used in previous literature. Where formal names are available these are given, else the GOODS team ‘nickname’ is presented for ease of comparison with previous work. For details of the sample see Dahlen et al. (2012), see also Svensson et al. (2010) for further analysis of these sources. Note that only objects with redshifts between $z = 0.35$ and $z = 1.35$ contribute to the stacks described in section 5.2. Six supernova host galaxies are individually detected at better than 3σ , with the strongest two detections both lying at the low redshift end of the sample. The remaining objects do not represent individual detections at the supernova location.

ID	RA & Declination (J2000)	Redshift	Flux μJy	RMS μJy	S/N
2002fz	03 32 48.566 -27 54 17.73	0.838	6.9	7.9	0.9
2002hq	03 32 30.027 -27 43 47.40	0.669	10.3	9.1	1.1
2002hs	03 32 18.537 -27 48 34.14	0.388	-3.8	7.6	-0.5
2002ke	03 31 58.677 -27 45 00.32	0.577	8.5	7.6	1.1
2002kb	03 32 42.429 -27 50 25.15	0.578	26.9	6.8	3.9
2002kl	12 37 49.281 62 14 06.61	0.412	5.6	6.0	0.9
2003ba	12 36 15.912 62 12 37.70	0.286	9.7	3.9	2.5
2003bb	12 36 24.423 62 08 36.58	0.955	8.0	4.4	1.8
2003bc	12 36 38.210 62 09 53.78	0.511	4.7	4.0	1.2
2003dx	12 36 31.681 62 08 48.66	0.512	5.7	5.0	1.1
2003dz	12 36 39.921 62 07 52.56	0.48	2.7	3.8	0.7
2003en	12 36 33.149 62 13 47.66	0.54	-0.81	4.0	-0.2
2003er	12 36 32.384 62 07 34.48	0.595	15.5	4.1	3.8
2003et	12 35 55.862 62 13 33.13	1.296	8.4	3.7	2.3
2003ew	12 36 27.806 62 11 25.07	0.517	5.1	4.0	1.3
2003N	12 37 09.265 62 11 00.65	0.425	3.0	6.3	0.5
K0404-005	12 36 27.056 62 15 09.75	0.79	-1.4	3.8	-0.4
K0404-006	12 37 06.731 62 21 17.82	0.406	4.0	4.4	0.9
K0404-008	12 38 03.647 62 17 11.77	0.278	69.0	3.9	17.5
K0404-010	12 36 46.069 62 16 25.80	0.61	-2.2	5.3	-0.4
K0404-011	12 36 49.362 62 16 04.83	1.53	1.9	4.0	0.5
K0405-001	12 35 50.757 62 10 37.95	1.012	5.6	3.8	1.5
K0405-002	12 36 26.710 62 08 30.15	0.556	0.40	4.4	0.1
K0405-005	12 36 35.991 62 17 32.67	0.683	-0.12	4.1	-0.03
K0405-007	12 36 58.447 62 16 37.37	0.497	-1.2	4.0	-0.3
K0405-008	12 37 33.842 62 19 22.24	0.88	2.3	5.0	0.5
HST04Bon	03 32 16.164 -27 49 41.81	0.664	34.0	6.9	4.9
HST04Cli	03 32 05.073 -27 41 42.61	0.75	6.82	7.1	1.0
HST04Con	12 37 08.258 62 12 53.74	0.838	6.1	3.9	1.6
HST04Cum	12 37 18.453 62 10 50.72	0.972	4.8	3.8	1.2
HST04Fox	03 32 41.765 -27 53 29.45	0.69	11.8	6.8	1.7
HST04Geo	12 36 44.432 62 10 53.19	0.937	2.2	4.2	0.5
HST04Gua	12 37 36.423 62 16 27.12	1.26	3.3	4.0	0.8
HST04Hei	03 32 42.415 -27 50 21.76	0.576	4.9	7.0	0.7
HST04Jef	03 32 23.679 -27 53 27.67	0.964	10.0	6.3	1.6
HST04Ken	03 32 44.702 -27 49 22.77	0.522	13.0	6.0	2.2
HST04Mur	03 32 35.307 -27 49 39.95	1.79	3.5	6.5	0.5
HST04Pata	12 37 25.258 62 10 06.36	0.41	32.4	4.1	8.0
HST04Patu	12 38 08.961 62 18 47.39	0.571	4.5	4.4	1.0
HST04Pol	03 32 19.681 -27 50 23.53	0.561	8.6	6.8	1.3
HST04Riv	03 32 32.407 -27 44 52.84	0.606	8.6	6.4	1.3
HST04Sos	03 32 22.638 -27 50 15.30	0.55	4.6	5.5	0.8
HST04Tov	03 32 49.625 -27 55 34.73	1.83	10.7	6.7	1.6
HST04Wil	03 32 13.061 -27 42 04.92	0.422	-6.9	7.2	-0.9
HST05Boy	03 32 44.859 -27 54 11.25	0.66	-10.6	7.3	-1.5
HST05Bra	12 37 21.764 62 12 25.67	0.48	10.4	4.9	2.2
HST05Cas	12 36 07.767 62 13 08.63	0.73	2.43	3.9	0.6
HST05Den	12 37 14.773 62 10 32.61	0.971	5.2	4.3	1.2
HST05Fil	12 37 19.329 62 15 59.30	1.21	2.9	4.0	0.7
HST05Kir	12 36 14.875 62 12 53.07	0.448	6.3	3.9	1.6
HST05Mob	12 36 25.518 62 15 11.04	0.68	1.3	3.6	0.4
HST05Pic	12 37 37.965 62 12 43.95	0.911	4.0	4.1	1.0
HST05Sco	12 36 51.196 62 19 56.11	0.93	-7.6	4.2	-1.8
HST05Sev	12 37 43.773 62 14 38.11	0.96	4.6	4.0	1.2
HST05Ste	12 37 01.534 62 17 47.13	0.475	3.5	4.5	0.8
HST05Str	12 36 46.879 62 11 45.21	1.06	2.3	4.3	0.6
HST05Ton	12 37 01.545 62 11 29.01	0.778	16.4	4.2	3.9

Table A1. Measured 1.4GHz data at the location of the core collapse supernovae discussed in this paper. Fluxes are measured on the VLA data obtained as part of the GOODS programme as described in the text. Targets are ordered by identifier name (broadly equivalent to ordering by date). Transients identified during the 2002-2003 observing campaign were reported by Strolger et al. (2004). Sources from 2004-2005 were classified by and discussed in Dahlen, Strolger, & Riess (2008) and Dahlen et al. (2012). The ID column refers to either the IAU transient name if assigned or the identifier assigned to the objects by the GOODS survey team, and used in previous literature (e.g. Svensson et al. 2010), to allow for straightforward comparison. The fifth column gives the rms of the local noise in the image for each object, and the sixth column the measured signal-to-noise at the supernova location. Six objects, marked with an asterisk, are individually detected.